A memristive non-smooth dynamical system with coexistence of bimodule periodic oscillation

Yang Yang[1], Minglin Ma[1,*], Zhijun Li[1], Mengjiao Wang[1],

Yichuang Sun[2], Liang Chen[1]

1. *School of Automation and Electronic Information, Xiangtan University, Xiangtan, Hunan 411105, P.R.China*

2. *School of Engineering and Technology, University of Hertfordshire, Hatfield AL10 9AB, UK*

Abstract: In order to explore the bursting oscillations and the formation mechanism of memristive non-smooth systems, a third-order memristor model and an external periodic excitation are introduced into a non-smooth dynamical system, and a novel 4D memristive non-smooth system with two-timescale is established. The system is divided into two different subsystems by a non-smooth interface, which can be used to simulate the scenario where a memristor encounters a non-smooth circuit in practical application circuits. Three different bursting patterns and bifurcation mechanisms are analyzed with the time series, the corresponding phase portraits, the equilibrium bifurcation diagrams, and the transformed phase portraits. It is pointed that not only the stability of the equilibrium trajectory but also the non-smooth interface may influence the bursting phenomenon, resulting in the sudden jumping of the trajectory and non-smooth bifurcation at the non-smooth interface. In particular, the coexistence of bimodule periodic oscillations at the non-smooth interface can be observed in this system. Finally, the correctness of the theoretical analysis is well verified by the numerical simulation and Multisim circuit simulation. This paper is of great significance for the future analysis and engineering application of the memristor in non-smooth circuits.

Keywords: Bursting oscillation; Non-smooth bifurcation; Non-smooth interface; Memristor; Bimodule periodic oscillation

1 Introduction

Multi-timescale systems have a wide range of practical application backgrounds, such as neuron firing models, the coupling effect of different transmission wires, and the reaction rates of different substances in chemical reactions [1-5], etc. Bursting oscillations are complex dynamical behaviors prevalent in multi-timescale systems, which are characterized by alternating large-scale oscillations and micro-scale oscillations [6-8]. When the system trajectory shows a large-amplitude oscillation, it corresponds to the spiking state, and when the system trajectory shows a micro-amplitude oscillation or almost constant, it corresponds to the quiescent state. Then the special bursting oscillations are formed when the system trajectory transitions between the spiking state and the quiescent state. There has been a lack of theoretical analysis methods for multi-timescale systems

* corresponding author.
E-mail address: minglin_ma@xtu.edu.cn

until Rinzel et al. [9] proposed the fast-slow analysis method, which elevates the bursting oscillation to the level of mechanism analysis. Therefore, the bursting oscillation system can be viewed as a dynamic system containing an internal variable governing its dynamic behavior. And similar systems also include Bouc-Wen type hysteresis responses [10], Dahl models [11], Saint-Venant elements [12], etc., and their internal variables represent different mechanisms.

In recent years, scholars have carried out in-depth research on bursting oscillations of various dynamical systems by the fast-slow analysis method, and have achieved a series of results. For example, Bao et al. [13] revealed chaotic bursting oscillations and the generation mechanism of the two fast and one slow Morris-Lecar neuron model, and verified the correctness of the theoretical analysis from the hardware circuit; Proskurkin et al. [14] studied the bursting oscillation phenomenon in chemical reaction systems; Han et al. [15] studied the bursting behavior of the parameter-excited Lorenz system and reported the chaotic bursting phenomenon caused by the bifurcation delay and chaotic crisis; Ma et al. [16] revealed the complex bursting structure induced by delayed pitchfork bifurcation in the periodically excited Jerk circuit; Han et al. [17] revealed two novel bursting oscillation patterns induced by turnover-pitchfork-hysteresis and compound-pitchfork by introducing multi-frequency parameter excitation in the Duffing oscillator; Wei et al. [18] studied the bursting dynamics behavior of mechanical systems under the combination of parametric excitation and external excitation, and revealed the complex cascaded bursting pattern caused by Hopf bifurcation and homoclinic bifurcation. On the other hand, bursting oscillations and their formation mechanism in non-smooth systems based on fast-slow analysis methods have also received extensive attention. For example, Li et al. [19] explored the existing conditions and generation mechanism of the possible bursting phenomenon in piecewise mechanical systems with different time scales. Zhang et al. [20] and Peng et al. [21] discussed the bursting oscillation behavior and its generation mechanism in the non-smooth Filippov system, and found the periodic smooth Fold/non-smooth Fold bursting, symmetric point-point type Fold/Fold-sliding bursting, symmetric point-cycle-cycle type Hopf/Hopf/Fold-sliding bursting. Then, Qu et al. [22] further investigated a more complex double excitation non-smooth Filippov system and discovered the multi-sliding bifurcation oscillation phenomenon. And Zhang et al. [23] found that introducing a non-smooth factor into the chaotic geomagnetic field model can lead to the phenomenon of grazing-sliding bifurcation and cross-sliding bifurcation. In addition, Leutcho et al. [24,25] studied chaotic hyperjerk circuits and revealed the phenomenon of mixed-mode bursting oscillations and various coexisting Feigenbaum remerging trees.

Furthermore, the use of memristors to simulate biological synapses in neural network hardware circuits has also received extensive attention due to its unique nonlinearity and memory effects in recent years [26-29]. For example, Ding et al. [30] investigated cortical signal propagation and the resulting spatiotemporal patterns in memristor-based neuronal network; Chen et al. [31] studied the bursting mechanism of memristive FitzHugh-Nagum circuits by using a graphical method; Lin et al. [32, 33] studied the multi-stable memristor and its application in neural network circuits; and in the review of the literature [34], the research progress of memristors in the chaos, memory and neural network circuits is briefly described. Wen et al. [35] introduced a smooth memristor model in the Jerk circuit and studied the bursting oscillation patterns under periodic parameter excitation. To the best of our knowledge, few studies have been reported on the bursting oscillations in the memristor-based non-smooth dynamical system.

Although the nonlinear dynamics based on the memristive system has attracted widespread

attention in the world in recent years, the study of bursting oscillation in the memristive non-smooth dynamical system still needs further exploration. Due to the existence of various non-smooth interfaces in the non-smooth system, the trajectory of the memristive non-smooth dynamical system has some special traversing forms when it passes through the non-smooth interfaces, which leads to the complex dynamic behavior of the system. Thus, the bursting oscillation behavior in memristor-based non-smooth dynamical systems is worth investigating. In order to reveal the bursting dynamics of memristive non-smooth system, this paper establishes a two-timescale 4D memristive non-smooth system according to the theoretical basis of [36]. This system can be used to simulate the scenario where a memristor encounters a non-smooth circuit in practical application circuits. Bursting oscillations of the system can be observed when an order gap exists between the excitation frequency and the natural frequency. Furthermore, the bursting oscillation and its formation mechanism are revealed in this study according to the differential inclusion theory. It is found that the sudden jumping of the system trajectory and non-smooth bifurcation at the non-smooth interface can cause the bursting oscillations of the system. And the coexistence of bimodule periodic oscillations at the non-smooth interface can be observed in this system.

The rest of this paper is organized as follows. In Sect. 2, a mathematical model of memristive non-smooth system is constructed. Sect. 3 analyzes the stability and bifurcation of the system. Sect. 4 discusses three different bursting oscillations and the corresponding bifurcation mechanism under different parameters. In Sect. 5, circuit simulation results are obtained. Finally, the conclusion of the paper is summarized in Sect. 6.

2 Mathematical model

This paper uses a third-order magnetron memristor, its model is obtained as

$$\begin{cases} i = k(\varphi^2 - 1)v \\ \dfrac{d\varphi}{dt} = -m\varphi^3 + n\varphi + pv \end{cases} \tag{1}$$

where i is the current of the memristor, v is the input voltage of the memristor, φ represents the internal state variable of the memristor, k is the coupling coefficient of the memristor and m, n, p are three memristive parameters. In this paper, we set $m = 1$, $n = 7$ and $p = 5$.

And the classical three-dimensional non-smooth Filippov model [37, 38] is

$$\begin{cases} \dfrac{dx}{dt} = 1 - uy + \alpha y^3 \\ \dfrac{dy}{dt} = \beta x - a_1 y \\ \dfrac{dz}{dt} = u(x - k_0 y) - (\beta - a)y + \beta z + k_0 \end{cases} \tag{2}$$

where $u = [1+sign(z)]/2$ represents the dimensionless switch controller, and α, β, a, a_1, k_0 are regarded as system parameters.

Then by introducing the third-order magnetron memristor into the above three-dimensional non-smooth dynamic system, a novel 4D memristive non-smooth dynamical system is constructed and can be described as

$$\begin{cases} \dfrac{dx}{dt} = 1 - uy + \alpha y^3 + \gamma \\ \dfrac{dy}{dt} = \beta x - k(w^2 - 1)y \\ \dfrac{dz}{dt} = u(x - k_0 y) - (\beta - a)y + \beta z + k_0 \\ \dfrac{dw}{dt} = -w^3 + 7w + 5y \end{cases} \tag{3}$$

where x, y, z are system state variables, w is the internal state variable of the memristor, $u = [1+sign(z)]/2$ is the segmented control item, and α, β, a, k_0 are regarded as system parameters. A slowly changing sinusoidal excitation is introduced into the control parameter γ, that is, $\gamma = A\sin(\Omega t)$, where A and Ω represent the amplitude and frequency of the parameter excitation, respectively.

When $0 < \Omega << 1$, there is a magnitude difference between the natural frequency of the system and the parameter excitation frequency in the system (3), which leads to the emergence of fast-slow effect. Therefore, the system (3) can be regarded as a classic fast-slow system and can be transformed into two subsystems: the slow subsystem (SS) is described by the $\gamma' = A\Omega\cos(\Omega t)$ and the fast subsystem (FS) is described by the system (3). When the SS is used to modulate the FS and the appropriate coupling coefficient k_0 is selected, the memristive non-smooth dynamic system will generate a variety of different bursting oscillation patterns. In the following, bursting oscillation patterns and the corresponding bifurcation mechanism will be discussed by using XPPAUT and MATLAB in detail.

3 Bifurcation and stability

According to the fast-slow analysis method, the periodic AC excitation $\gamma = A\sin(\Omega t)$ can be regarded as a slow-varying parameter in the FS. Due to the existence of the segmented control item u, the system is divided into two different subsystems, denoted as FS_- and FS_+, respectively described as

$$FS_-: \begin{cases} \dot{x} = 1 + \alpha y^3 + \gamma \\ \dot{y} = \beta x - k(w^2 - 1)y \\ \dot{z} = -(\beta - a)y + \beta z + k_0 \\ \dot{w} = -w^3 + 7w + 5y \end{cases} \tag{4}$$

$$FS_+: \begin{cases} \dot{x} = 1 - y + \alpha y^3 + \gamma \\ \dot{y} = \beta x - k(w^2 - 1)y \\ \dot{z} = (x - k_0 y) - (\beta - a)y + \beta z + k_0 \\ \dot{w} = -w^3 + 7w + 5y \end{cases} \tag{5}$$

Suppose the equilibrium points of the two subsystems are set as $E_- = (x_1, y_1, z_1, w_1)$, $E_+ = (x_2, y_2, z_2, w_2)$ respectively, and the FS_- is linearized at the equilibrium point E_-, then the corresponding Jacobian matrix is obtained as

$$J_{-}=\begin{pmatrix}0 & 3\alpha y_1^{\,2} & 0 & 0\\ \beta & -k(w_1^2-1) & 0 & -2kw_1y_1\\ 0 & -\beta+a & \beta & 0\\ 0 & 5 & 0 & -3w_1^2+7\end{pmatrix} \tag{6}$$

Thus, the characteristic equation corresponding to the Jacobian matrix J_{-} may be written as

$$\begin{aligned} f(\lambda) &= |\lambda \mathrm{I}-J_{-}| \\ &= \lambda^4+P_1\lambda^3+P_2\lambda^2+P_3\lambda+P_0=0 \end{aligned} \tag{7}$$

where
$$\begin{cases} P_1 = kw_1^2-\beta-k+3w_1^2-7 \\ P_2 = 10kw_1y_1+k\beta-kw_1^2\beta-3\alpha\beta y_1^{\,2}+(3w_1^2-7)(kw_1^2-\beta-k) \\ P_3 = -10k\beta w_1y_1+3\alpha\beta^2 y_1^{\,2}+(3w_1^2-7)(k\beta-kw_1^2\beta-3\alpha\beta y_1^{\,2}) \\ P_0 = 9\alpha\beta^2w_1^2y_1^{\,2}-21\alpha\beta^2y_1^2 \end{cases}$$

According to the Routh-Hurwitz theory, the equilibrium points E_{-} are stable for

$$P_1>0,\ (P_1P_2-P_3)>0,\ P_3+P_3P_0-P_1P_2P_0>0 \tag{8}$$

When the slow-varying parameter γ changes periodically, the stable conditions of the equilibrium point E_{-} are invalid, leading to the fold bifurcation [39, 40] and Hopf bifurcation.

(1) Fold bifurcation

$$P_0=9\alpha\beta^2w_1^2y_1^{\,2}-21\alpha\beta^2y_1^2=0 \tag{9}$$

(2) Hopf bifurcation

$$P_0=0,\ P_1P_2-P_3=0 \tag{10}$$

Similarly, the FS_{+} is linearized at the equilibrium point E_{+}, then the corresponding Jacobian matrix is obtained as

$$J_{+}=\begin{pmatrix}0 & -1+3\alpha y_2^{\,2} & 0 & 0\\ \beta & -k(w_2^2-1) & 0 & -2kw_2y_2\\ 1 & -k_0-\beta+a & \beta & 0\\ 0 & 5 & 0 & -3w_2^2+7\end{pmatrix} \tag{11}$$

Thus, the characteristic equation corresponding to the Jacobian matrix J_{+} may be written as

$$\begin{aligned} f(\lambda) &= |\lambda \mathrm{I}-J_{+}| \\ &= \lambda^4+Q_1\lambda^3+Q_2\lambda^2+Q_3\lambda+Q_0=0 \end{aligned} \tag{12}$$

where
$$\begin{cases} Q_1 = kw_2^2-\beta-k+3w_2^2-7 \\ Q_2 = 10kw_2y_2+k\beta-kw_2^2\beta+\beta-3\alpha\beta y_2^{\,2}+(3w_2^2-7)(kw_2^2-\beta-k) \\ Q_3 = -10k\beta w_2y_2+3\alpha\beta^2y_2^{\,2}-\beta^2+(3w_2^2-7)(k\beta-k\beta w_2^2+\beta-3\alpha\beta y_2^{\,2}) \\ Q_0 = (3w_2^2-7)(3\alpha\beta^2y_2^{\,2}-\beta^2) \end{cases}$$

According to the Routh-Hurwitz theory, the equilibrium points E_{+} are stable for

$$Q_1 > 0,\ (Q_1Q_2 - Q_3) > 0,\ Q_3 + Q_3Q_0 - Q_1Q_2Q_0 > 0 \tag{13}$$

When the slow-varying parameter γ changes periodically, the stable conditions of the equilibrium point E_+ are invalid, leading to the following two different bifurcations.

(1) Fold bifurcation

$$Q_0 = (3w_2^2 - 7)(3\alpha\beta^2 y_2^{\ 2} - \beta^2) = 0 \tag{14}$$

(2) Hopf bifurcation

$$Q_0 = 0,\ Q_1Q_2 - Q_3 = 0 \tag{15}$$

At the non-smooth interface {NS: Z=0}, the equilibrium point of the system is set as $E_0 = (x_0, y_0, 0, w_0)$, and the characteristic equation corresponding to the generalized Jacobian matrix is

$$\lambda^4 + N_1\lambda^3 + N_2\lambda^2 + N_3\lambda + N_0 = 0 \tag{16}$$

According to the differential inclusion theory [41], the auxiliary parameter q ($q \in [0, 1]$) is introduced to combine the two subsystems FS- and FS+ and $N_i = qQ_i + (1-q)P_i$, $i = 0, 1, 2, 3$ can be obtained. As the auxiliary parameter q varies, the associated eigenvalues may pass across the real axis or the pure imaginary axis, leading to possible non-smooth bifurcations. Therefore, the following two different bifurcations may be produced.

(1) Non-smooth fold bifurcation (NSFB)

$$N_0 = 0 \tag{17}$$

(2) Non-smooth Hopf bifurcation (NSHB) [42, 43]

$$N_0 = 0,\ N_1N_2 - N_3 = 0 \tag{18}$$

When the system parameters are fixed at $\alpha = 2$, $\beta = -8$, $a = 2$, $k_0 = 4$; $A = 2$, $\Omega = 0.005$, and the coupling coefficient k is variable, the bursting oscillation patterns of the system are studied. And the corresponding Lyapunov exponent spectrum of the system state variable is illustrated in Fig. 1. The Jacobian matrix algorithm is applied for computing the Lyapunov exponent spectrum (LEs) and the number of time series for computing LEs is 40,000. It can be clearly seen that in the whole varying range of k, the maximum LE of system is negative, indicating that the system is in a stable state and there is no chaotic state.

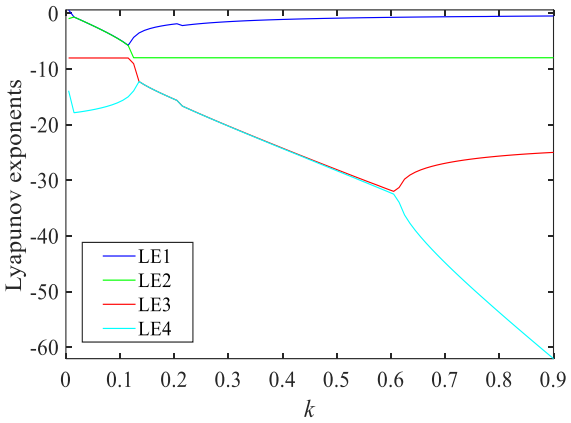

Fig. 1. LEs of the system state variable with $\alpha = 2$, $\beta = -8$, $a = 2$, $k_0 = 4$, $A = 2$, $\Omega = 0.005$ and different $k = [0, 0.9]$.

4 Bursting oscillations mechanisms

In this section, we consider the situation that the coupling coefficient k is variable and all the other system parameters are fixed. The following three typical bursting oscillation patterns with the parameter $k = 0.2, 0.3, 0.4$ are studied respectively. In order to explore the bursting phenomena and the corresponding formation mechanism of the memristive non-smooth dynamical system, the effect of the coupling coefficient k on bursting dynamics is analyzed by the time series, the corresponding phase portraits, the equilibrium bifurcation diagrams, and the transformed phase portraits.

4.1 Case 1: $k = 0.2$

Taking the parameter $k = 0.2$, and the slow-varying parameter γ varies between –2 and 2. In this case, when γ reaches the critical value of the bifurcation point, the corresponding dynamic behavior may occur. To reveal the bifurcation mechanism of bursting oscillation, the equilibrium bifurcation diagram and the transformed phase portrait on γ-z plane are shown in Fig. 2(a) and (b), respectively.

Due to the existence of segmented control item $u = [1+sign(z)]/2$, the system is divided into two sub-regions: FS_- ($z<0$) and FS_+ ($z>0$). In each sub-region, the trajectory of the system is separately controlled by the respective subsystem. In the area D_-, the equilibrium points E_- plays a control role, and the E_- is divided into E_1^- and E_2^- due to the existence of the interface NS. Similarly, the equilibrium points E_+ is divided into E_1^+, E_2^+, E_3^+ and E_4^+. In Fig. 2(a), the red curves represent the achievable equilibrium points, namely E_1^+, E_2^+, E_3^+ and E_1^-, the black curves represent the unachievable equilibrium points, namely E_4^+ and E_2^-, the solid lines represent the stable equilibrium points, the dashed line represents the unstable equilibrium points. The NH1 and NH2 represent the non-smooth Hopf bifurcation points at the interface, the green LC_s represents the stable limit cycle generated by the fold limit cycle, and the blue LC_u represents the unstable limit cycle. Then, the transformed phase portrait on the γ-z plane is shown in Fig. 2(b). It can be seen that the trajectory includes three quiescent states (QSs) and three spiking states (SPs) in one motion cycle.

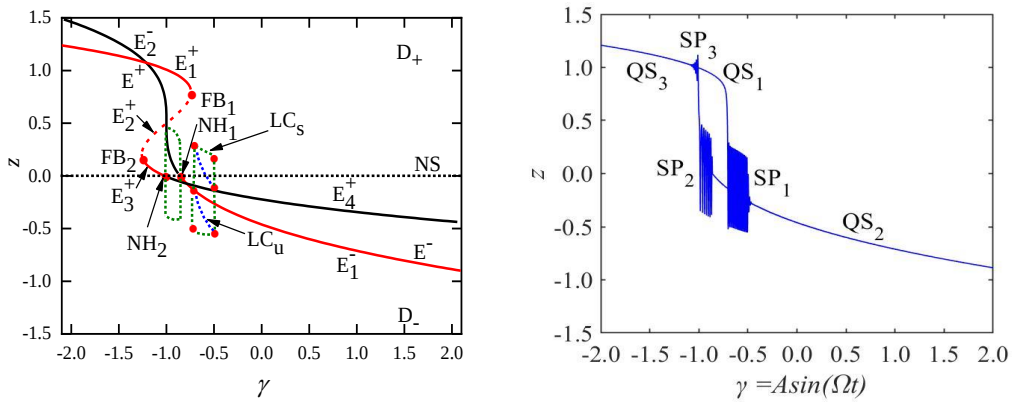

(a) **(b)**

Fig. 2. When $k = 0.2$, $\alpha = 2$, $\beta = -8$, $a = 2$, $k_0 = 4$, $A = 2$, $\Omega = 0.005$, **(a)** the equilibrium bifurcation diagram, **(b)** the transformed phase portrait on the γ-z plane.

Fig. 3(a) shows the phase portrait on the x-z plane when $k = 0.2$. It can be clearly seen that the trajectory of the system includes two periodic oscillations and a part that rapidly converges to the equilibrium point, where the red arrows are the motion directions of the trajectory between different attractors. Fig. 3(b) is the time series diagram of the state variable z, Fig. 3(c) is a local enlarged view of the periodic oscillation on the left side of Fig. 3(b), and Fig. 3(d) is a local enlarged view of the periodic oscillation on the right side of Fig. 3(b). It can be intuitively seen that the motion trajectory has obvious non-smooth characteristics when it crosses the interface NS. That is, there is the coexistence of dual-mode periodic oscillations at the non-smooth interface. In addition, it should be pointed out that the mechanism of the two non-smooth bifurcations is different. The phenomenon in Fig. 3(c) is due to the limit cycle generated by the non-smooth Hopf bifurcation at the interface NS, while the phenomenon in Fig. 3(d) is due to fold limit cycle generated by the alternate control of the two subsystems when the trajectory of the system crosses the interface NS back and forth.

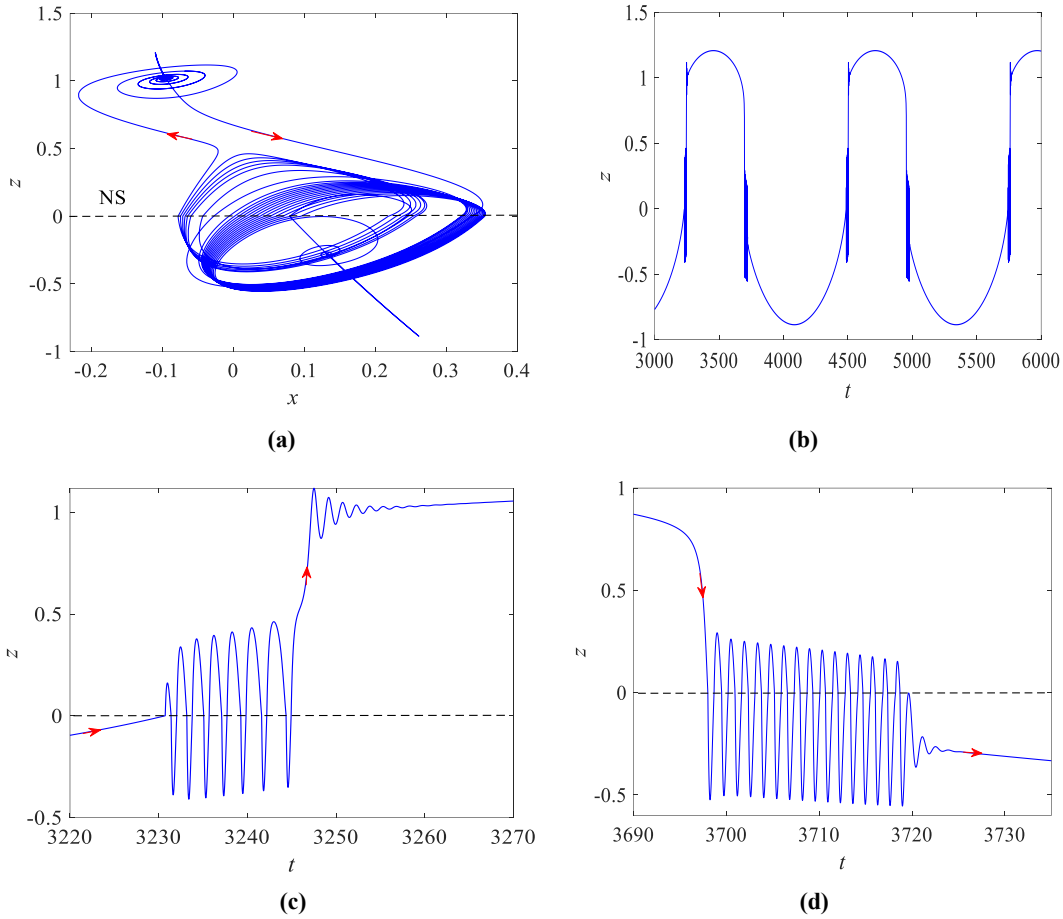

Fig. 3. When $k = 0.2$, $\alpha = 2$, $\beta = -8$, $a = 2$, $k_0 = 4$, $A = 2$, $\Omega = 0.005$, (**a**) the phase portrait on the x-z plane, (**b**) the time series diagram of the state variable z, (**c**) a local enlarged view on the left side of the state variable z, (**d**) a local enlarged view on the right side of the state variable z.

In order to further illustrate the transition mechanism of these trajectories between different equilibrium points, Fig. 4 shows the superimposed diagram of the equilibrium bifurcation diagram and the transformed phase portrait on the γ-z plane. Assuming that the trajectory starts from the point P_1, the slow variable takes the minimum value $\gamma = -2$ at this time. Since the stable equilibrium point curve E_1^+ and the control subsystem FS_+ are both located in D_+, the trajectory strictly follows the movement of E_1^+, forming the quiescent state QS_1. Then it moves to the fold bifurcation point FB_1, jumps down from the FB1, bounces back to D_+ due to the excessive jump amplitude, and then jumps back and forth to form the spiking state SP_1. When the trajectory crosses the interface NS, the stability of the two subsystems is exchanged, and the system is controlled by the subsystem FS_- in the D_-. Due to the large jump at FB_1, the trajectory traverses back and forth at the interface and is controlled alternately by the two subsystems to generate the fold limit cycle bifurcation, that is, the non-smooth periodic bursting oscillation around NS. After the end of this oscillation, the trajectory quickly converges to the stable equilibrium point E_1^- of the control subsystem FS_- in the D_-, forming the quiescent state QS_2. Then it moves along E_1^- until the slow variable reaches the maximum value $\gamma = 2$, which is the point P_2 in Fig. 4. Then the slow variable starts to decrease in the opposite direction, and the trajectory moves along E_1^- again until it generates the non-smooth Hopf bifurcation at the interface NS, and the trajectory forms a non-smooth periodic bursting

oscillation around the interface, namely SP_2. At the end of this oscillation, the system trajectory jumps directly to E_1^+ controlled by FS_+ and slowly converges to E_1^+, forming the spiking state SP_3. Then it moves along E_1^+ to form the quiescent state QS_3. Until the slow variable returns to the minimum value again, that is, the trajectory returns to the point P_1, a cycle of movement is completed. In particular, the coexistence phenomenon of two periodic oscillations at the interface can be observed throughout the cyclic motion. Namely, the coexistence of bimodule periodic oscillations has been discovered at the interface of the memristor-based non-smooth system. According to the type of bifurcation, the dynamical behavior can be called as periodic fold/fold limit cycle/non-smooth Hopf bifurcation bursting. Geometrically, this bursting pattern is also the cycle-point-cycle-point type.

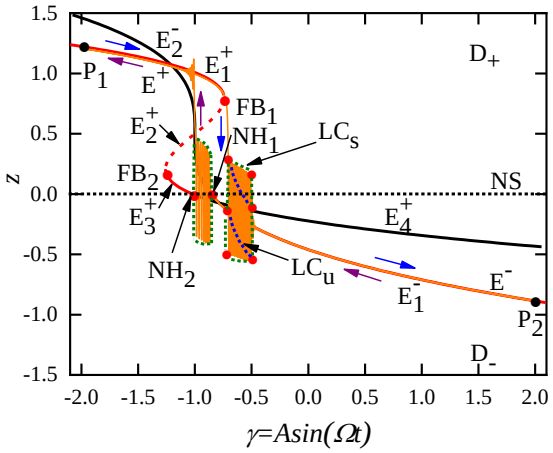

Fig. 4. When $k = 0.2$, $\alpha = 2$, $\beta = -8$, $a = 2$, $k_0 = 4$, $A = 2$, $\Omega = 0.005$, the superimposed diagram of the equilibrium bifurcation diagram and the transformed phase portrait on the γ-z plane.

4.2 Case 2: $k = 0.3$

Now we consider the parameter $k = 0.3$, and the slow-varying parameter γ varies between -2 and 2. To reveal the bifurcation mechanism of bursting oscillation, the equilibrium bifurcation diagram and the transformed phase portrait on γ-z plane are shown in Fig. 5(a) and (b), respectively. In this case, the trajectory includes three quiescent states (QSs) and three spiking states (SPs) in one motion cycle.

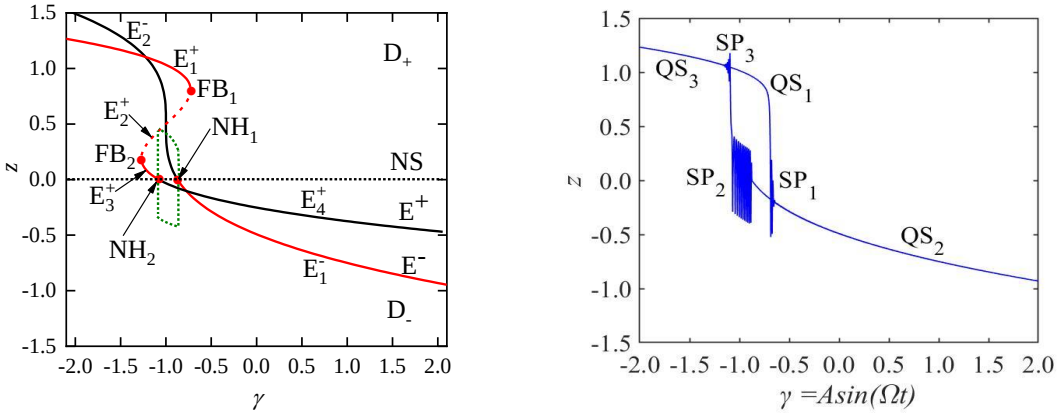

Fig. 5. When $k = 0.3$, $\alpha = 2$, $\beta = -8$, $a = 2$, $k_0 = 4$, $A = 2$, $\Omega = 0.005$, (**a**) the equilibrium bifurcation diagram, (**b**) the transformed phase portrait on the γ-z plane.

Fig. 6(a) shows the phase portrait on the x-z plane when $k = 0.3$. It can be clearly seen that the trajectory of the system includes three parts: one periodic oscillation and two parts that rapidly converges to the equilibrium point, where the red arrows are the motion directions of the trajectory between different attractors. Fig. 6(b) is the time series diagram of the state variable z, and Fig. 6(c) is a local enlarged view of the rapid convergence of Fig. 6(b) after crossing the interface. It can be intuitively seen that the motion trajectory has obvious non-smooth characteristics when it crosses the interface NS.

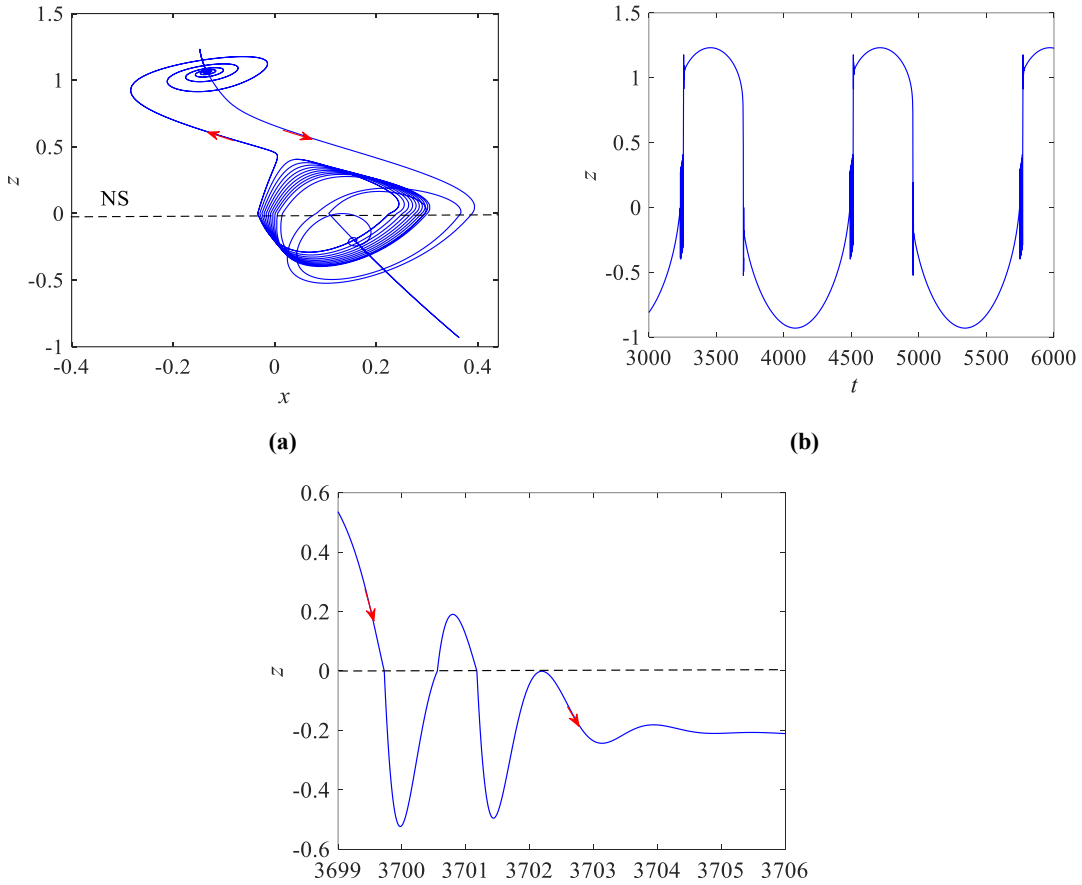

Fig. 6. When $k = 0.3$, $\alpha = 2$, $\beta = -8$, $a = 2$, $k_0 = 4$, $A = 2$, $\Omega = 0.005$, (**a**) the phase portrait on the x-z plane, (**b**) the time series diagram of the state variable z, (**c**) a local enlarged view on the right side of the state variable z.

In order to further illustrate the transition mechanism of these trajectories between different equilibrium points, Fig. 7 shows the superimposed diagram of the equilibrium bifurcation diagram and the transformed phase portrait on the γ-z plane. It is still assumed that the trajectory starts from the point P_1, which corresponds to the minimum value of the slow variable $\gamma = -2$. Since the stable equilibrium point curve E_1^+ and the control subsystem FS_+ are both located in D_+, the trajectory strictly follows the movement of E_1^+, forming the quiescent state QS_1. Then it moves to the fold bifurcation point FB_1, and jumps from the fold bifurcation to form the spiking state SP_1. When the trajectory crosses the interface NS, the trajectory quickly converges to the stable equilibrium point E_1^- of the control subsystem FS_- in the D_-, forming the quiescent state QS_2. Then it moves along E_1^- until the slow variable reaches the maximum value $\gamma = 2$, which is the point P_2 in Fig. 7. As the slow variable begins to decrease, the trajectory moves along E_1^- again until it encounters the NH2 point at the interface NS, resulting in a non-smooth Hopf bifurcation, and the trajectory forms a non-smooth periodic bursting oscillation around the interface, namely SP_2. As the oscillation ends, the system trajectory jumps directly to E_1^+ controlled by FS_+, forming the spiking state SP_3. Then it moves along E_1^+ to form the quiescent state QS_3. Until the slow variable returns to the minimum value again, the trajectory returns to the point P_1 to complete a cycle of movement. According to the type of bifurcation, the dynamical behavior can be called as periodic fold/non-smooth Hopf bifurcation bursting. Geometrically, this bursting pattern is also the point-cycle-point type.

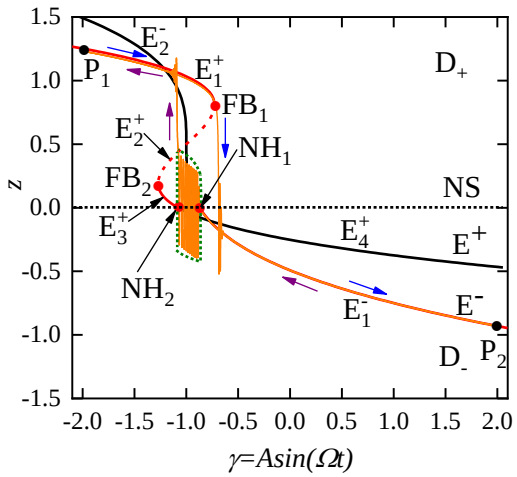

Fig. 7. When $k = 0.3$, $\alpha = 2$, $\beta = -8$, $a = 2$, $k_0 = 4$, $A = 2$, $\Omega = 0.005$, the superimposed diagram of the equilibrium bifurcation diagram and the transformed phase portrait on the γ-z plane.

4.3 Case 3: $k = 0.4$

Finally, we consider the parameter $k = 0.4$, and the slow-varying parameter γ varies between -2 and 2. To reveal the bifurcation mechanism of bursting oscillation, the equilibrium bifurcation diagram and the transformed phase portrait on γ-z plane are shown in Fig. 8(a) and (b), respectively. In this case, the trajectory includes four quiescent states (QSs) and three spiking states (SPs) in one motion cycle.

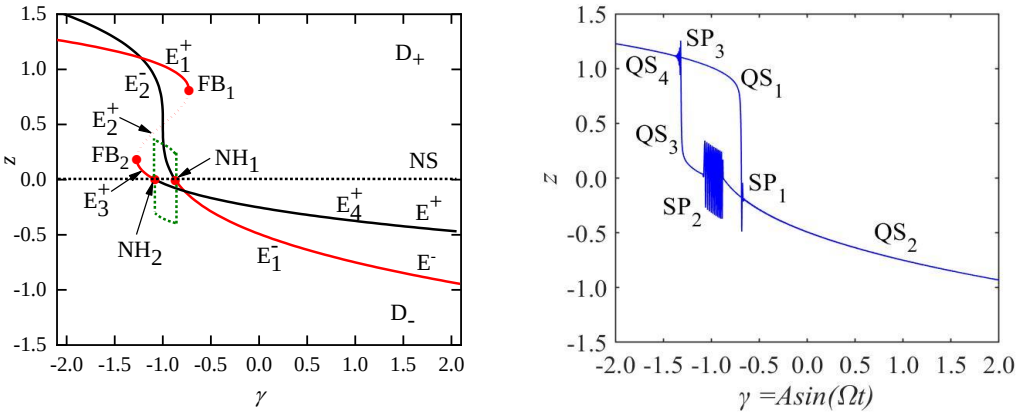

Fig. 8. When $k = 0.4$, $\alpha = 2$, $\beta = -8$, $a = 2$, $k_0 = 4$, $A = 2$, $\Omega = 0.005$, (**a**) the equilibrium bifurcation diagram, (**b**) the transformed phase portrait on the γ-z plane.

Fig. 9(a) shows the phase portrait on the x-z plane when $k = 0.4$. It can be clearly seen that the trajectory of the system includes three parts: one periodic oscillation and two parts that rapidly converges to the equilibrium point, where the red arrows are the motion directions of the trajectory between different attractors. Fig. 9(b) is the time series diagram of the state variable z, and Fig. 9(c) is a local enlarged view of the non-smooth periodic oscillation of Fig. 9(b). It can be intuitively seen that the motion trajectory has obvious non-smooth characteristics when it crosses the interface NS.

Here, the black arrows indicate the direction of the motion trajectory going up through the NS, and the red arrows indicate the direction of the motion trajectory going down through the NS.

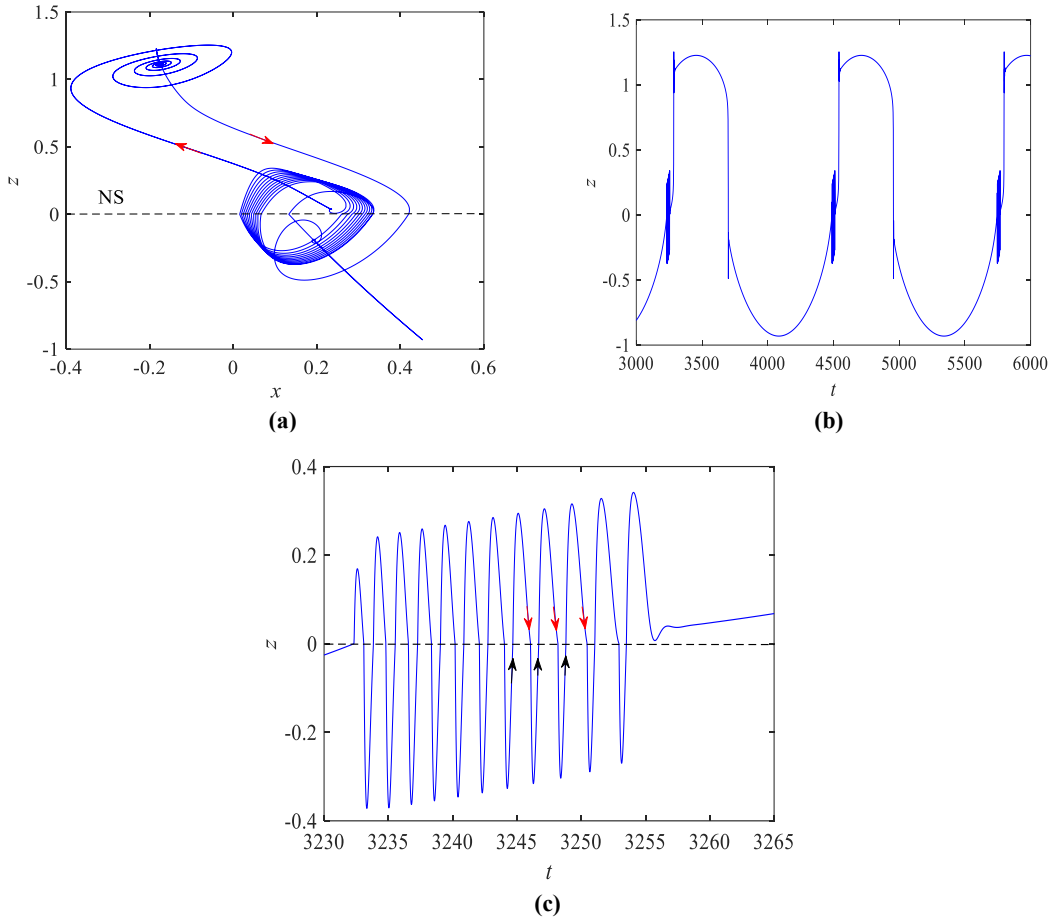

Fig. 9. When $k = 0.4$, $\alpha = 2$, $\beta = -8$, $a = 2$, $k_0 = 4$, $A = 2$, $\Omega = 0.005$, (**a**) the phase portrait on the x-z plane, (**b**) the time series diagram of the state variable z, (**c**) a local enlarged view on the left side of the state variable z.

Similarly, Fig. 10 shows the superimposed diagram of the equilibrium bifurcation diagram and the transformed phase portrait on the γ-z plane in order to further illustrate the transition mechanism of these trajectories between different equilibrium points. It is still assumed that the trajectory starts from the point P_1, which corresponds to the minimum value of the slow variable $\gamma = -2$. And the trajectory strictly follows the movement of E_1^+ to form the quiescent state QS_1. Then it moves to the fold bifurcation point FB_1, and jumps from the fold bifurcation to form the spiking state SP_1. When the trajectory crosses the interface NS, the trajectory quickly converges to the stable equilibrium point E_1^- of the control subsystem FS_- in the D_-, forming the quiescent state QS_2. Then it moves along E_1^- until the slow variable reaches the maximum value $\gamma = 2$, which is the point P_2 in Fig. 10. As the slow variable begins to decrease, the trajectory moves along E_1^- again until it encounters the NH2 point at the interface NS, resulting in a non-smooth Hopf bifurcation, and the trajectory forms a non-smooth periodic bursting oscillation around the interface, namely SP_2. As the oscillation ends, the system trajectory converges directly to the stable equilibrium point E_3^+ controlled by FS_+, forming the quiescent state QS_3. When it moves to the fold bifurcation point FB_2, the trajectory turns to E_1^+ to form the spiking state SP_3. Then it gradually converges to the stable equilibrium point E_1^+, forming the quiescent state QS_4. Until the slow variable returns to the minimum value again, the trajectory returns to the point P_1 to complete a cycle of movement. And

the dynamical behavior can be called as periodic fold/non-smooth Hopf bifurcation/fold bifurcation bursting. From the geometric structure, this bursting pattern is also the point-cycle-point-point type. In addition, it should be pointed out that this bursting pattern is caused by the different memristive coupled parameter values. It is shown that after the non-smooth Hopf periodic oscillation, the trajectory does not directly transfer to E_1^+ through a large jump like $k = 0.3$, but instead converges to a nearby stable equilibrium point E_2^+ when $k = 0.4$.

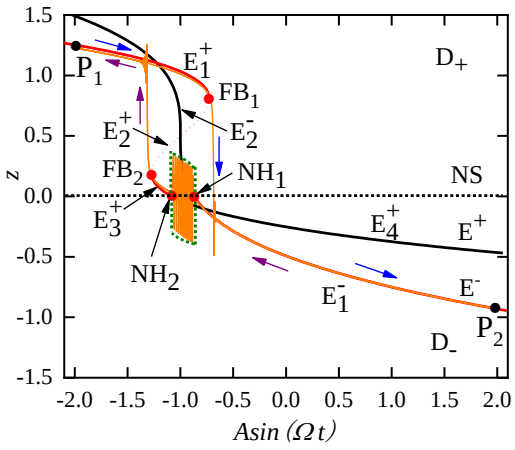

Fig. 10. When $k = 0.4$, $\alpha = 2$, $\beta = -8$, $a = 2$, $k_0 = 4$, $A = 2$, $\Omega = 0.005$, the superimposed diagram of the equilibrium bifurcation diagram and the transformed phase portrait on the γ-z plane.

5 Multisim circuit verification

Although a lot of research has been carried out to reveal the dynamics of bursting and explore the corresponding bifurcation mechanism numerically, there is little experimental validation on this issue. Furthermore, experimentally generating bursting oscillations from physical circuits is a meaningful topic because the generated bursting signals can be used to simulate biological signals in artificial devices such as pacemakers or neurons. In this section, the analog circuit of the memristive non-smooth dynamical system under periodic external excitation is designed to verify the bursting oscillations and the formation mechanism. As shown in Fig. 11, the complete circuit is constructed by the modular design method, and the system is driven by an external excitation $V_0 = A\sin(2\pi ft)$, where A is the excitation amplitude and f is the excitation frequency. In the circuit, the device used for the operational amplifiers is TL082CD and the device used for the multipliers is AD633AN. All active devices in the circuit are powered with ±12V supply voltages.

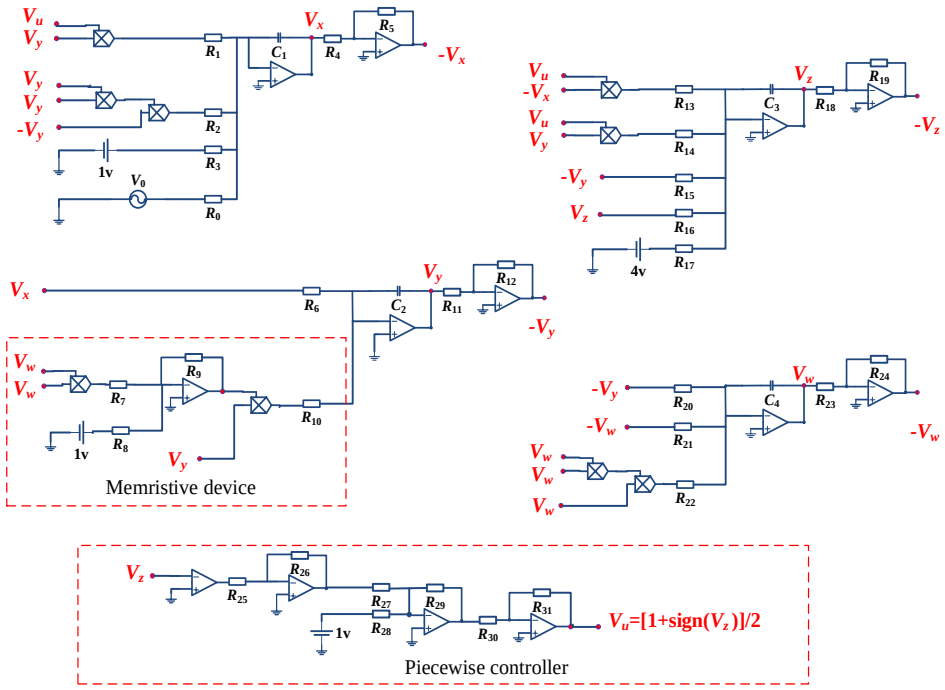

Fig. 11. Multisim simulation circuit of the memristive non-smooth dynamical system.

The memristive dynamical system we want to implement by the circuit in Fig.11 as example is given in (19).

$$\begin{cases} \dfrac{dx}{dt} = -(-100) - 100uy - 200yy(-y) + A\sin(\omega t) \\ \dfrac{dy}{dt} = -800x - 24(ww-1)y \\ \dfrac{dz}{dt} = -100u(-x) - 400uy - 1000(-y) - 800z - (-400) \\ \dfrac{dw}{dt} = -100ww(-w) - 700(-w) - 500(-y) \end{cases} \tag{19}$$

Applying Kirchhoff's circuit laws and setting the time conversion factor τ = 100, the obtained circuit equation can be written as

$$\begin{cases} \dfrac{dV_x}{dt} = -\dfrac{V_u V_y}{10R_1C_1} - \dfrac{V_y V_y(-V_y)}{100R_2C_1} - \dfrac{-V_1}{R_3C_1} + \dfrac{1}{R_0} A\sin(2\pi ft) \\ \dfrac{dV_y}{dt} = -\dfrac{V_x}{R_6C_2} - \dfrac{(V_wV_w-1)V_y}{100R_{10}C_2} \\ \dfrac{dV_z}{dt} = -\dfrac{V_u(-V_x)}{10R_{13}C_3} - \dfrac{V_uV_y}{R_{14}C_3} - \dfrac{-V_y}{R_{15}C_3} - \dfrac{V_z}{R_{16}C_3} - \dfrac{-V_2}{R_{17}C_3} \\ \dfrac{dV_w}{dt} = -\dfrac{-V_y}{R_{20}C_4} - \dfrac{-V_w}{R_{21}C_4} - \dfrac{V_wV_wV_w}{100R_{22}C_4} \end{cases} \tag{20}$$

where V_x, V_y, V_z, and V_w represent system variables x, y, z, and w, respectively. Therefore, by matching the circuit equation (20) with the expected equation (19), the values of circuit elements

can be obtained as illustrated in Table 1. It is worth noting that the system can be adapted to different cases by adjusting the value of resistor R_{10}.

Table 1

Circuit parameters of the proposed memristor-based circuit

Parameters	Significations	Values
$R_{0,3,8,9,23,24,29}$	Resistance	100kΩ
$R_{1,4,5,7,11,12,13,15,18,19,30,31}$	Resistance	10kΩ
R_2	Resistance	0.5kΩ
$R_{6,16}$	Resistance	12.5kΩ
R_{14}	Resistance	2.5kΩ
R_{17}	Resistance	25kΩ
R_{20}	Resistance	20kΩ
R_{21}	Resistance	14.28kΩ
$R_{22,26}$	Resistance	1kΩ
R_{25}	Resistance	13.5kΩ
$R_{27,28}$	Resistance	50kΩ
R_{10}	Resistance	Adjustable
$C_{1\text{-}4}$	Capacitance	10nF
V_0	Sinusoidal signal	Adjustable

Then, the circuit simulation results of the memristive non-smooth dynamical system are shown in Fig. 12. In Fig. 12 (a), (c), (e), the horizontal axis is 100ms per grid and the vertical axis is 500mV per grid. Then in Fig. 12 (b), (d), (f), the horizontal axis is 100mV per division and the vertical axis is 500mV per division. From Fig. 12, it can be found that the circuit simulation results are well consistent with the numerical simulation results shown in Fig. 3, Fig. 6 and Fig. 9. Thus, it is a good proof that the memristive non-smooth dynamical system does exhibit complex bursting dynamics when an order gap exists between the excitation frequency and the natural frequency.

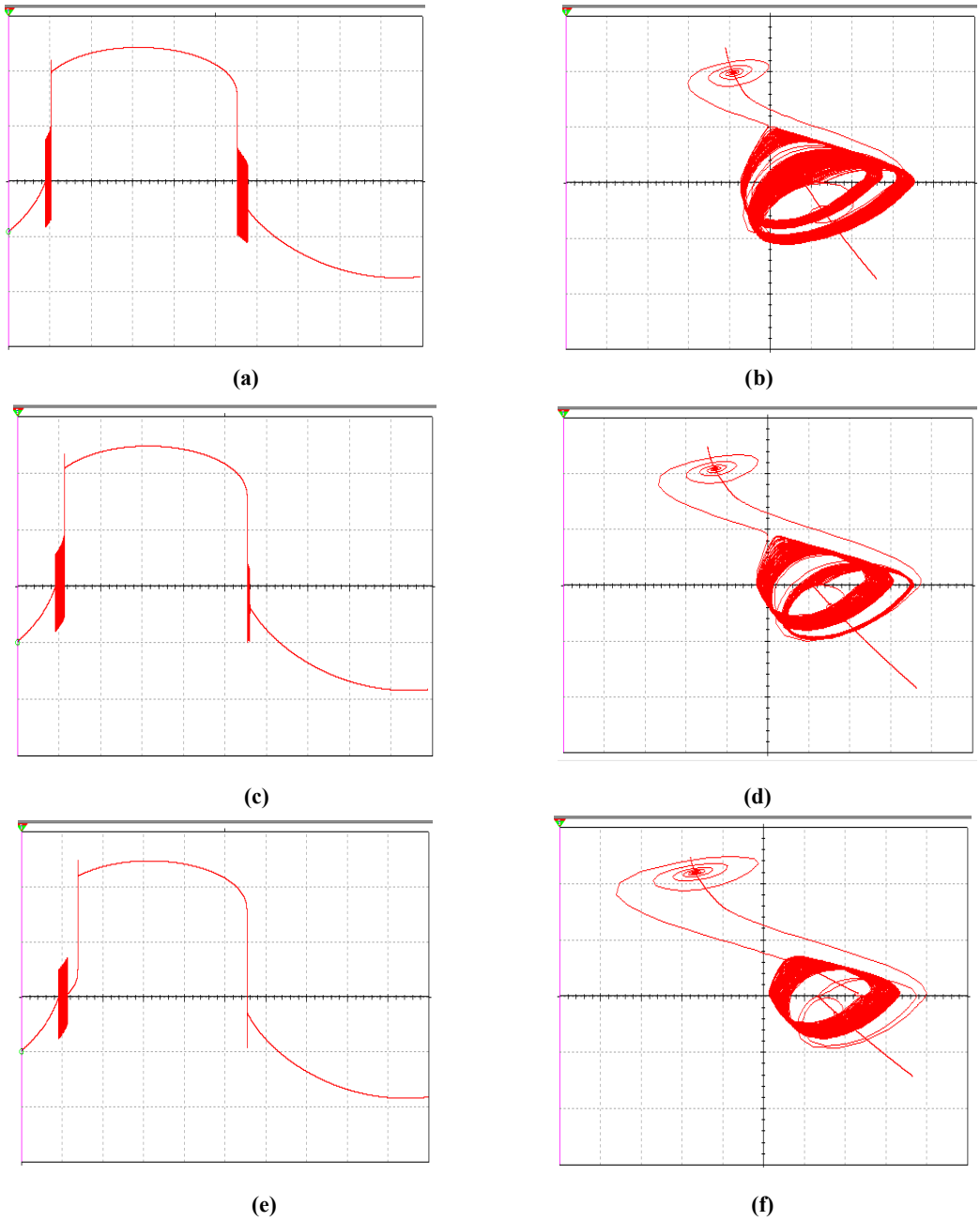

Fig. 12. Circuit simulation results of the memristive non-smooth dynamical system with $\alpha = 2$, $\beta = -8$, $a = 2$, $k_0 = 4$, $A = 2$, $\Omega = 0.005$ (**a**) the time series diagram of the state variable z with $k = 0.2$, (**b**) the phase portrait on the x-z with $k = 0.2$, (**c**) the time series diagram of the state variable z with $k = 0.3$, (**d**) the phase portrait on the x-z with $k = 0.3$, (**e**) the time series diagram of the state variable z with $k = 0.4$, (**f**) the phase portrait on the x-z with $k = 0.4$.

6 Conclusion

In this paper, a third-order memristor model and an external periodic excitation are introduced into a three-dimensional non-smooth dynamic system, and a novel 4D memristive non-smooth system is constructed to simulate the scenario where the memristor encounters a non-smooth circuit in practical application circuits. When the external periodic excitation frequency is much smaller than

the natural frequency of the system, the system can be regarded as a typical fast-slow system with two-timescale. The system is divided into two different sub-regions, and each sub-region has a corresponding control subsystem. When the trajectory of the system passes through the non-smooth interface of the two sub-regions, special dynamic behaviors will be generated. Based on MATLAB and XPPAUT numerical simulation and Multisim circuit simulation, three different bursting oscillation patterns and bifurcation mechanisms caused by different system parameter k are revealed. In addition, the coexistence of bimodule periodic oscillations at non-smooth interface is reported in this system. It should be noted that the mutual motion of the system between the spiking states and the quiescent states is not caused by the inherent bifurcation of the system like the continuous system, but is formed by the non-smooth bifurcation at the non-smooth interface and the change of the critical condition. In conclusion, the coexistence of bimodule periodic bursting oscillations at the non-smooth interface in the memristive non-smooth dynamical system is investigated for the first time in this paper, which further enriches the bursting oscillation path of the memristive dynamic system. And the next work should be bursting oscillations of non-smooth memristive systems with multiple slow variable excitations and their practical application.

Declaration of Competing Interest

The authors declare that they have no known competing financial interests or personal relationships that could have appeared to influence the work reported in this paper.

Acknowledgements This work was supported by the National Key Research and Development Program of China under Grant No.2018AAA0103300 and the National Natural Science Foundations of China under Grants No. 62171401 and 62071411.

Author contribution statement

All authors contributed equally to this work. YY wrote the main paper. MLM performed the MATLAB simulations. ZJL designed and implemented the simulation of the integrated circuit. MJW and YCS polished the manuscript. LC carried out the drawing of XPPAUT. All authors discussed the results and commented on the manuscript at all stages.

References

1. Zhang Z, Li Y, Bi Q. Routes to bursting in a periodically driven oscillator. Physics Letters A 2013;377(13):975-980.
2. Liepelt S, Freund JA, Schimansky-Geier L, et al. Information processing in noisy burster models of sensory neurons. Journal of Theoretical Biology 2005;237(1):30-40.
3. John HG, Macdonald, Guy LL. Two-degree-of-freedom inclined cable galloping. Journal of Wind Engineering and Industrial Aerodynamics 2008;96(3):291-307.
4. Proskurkin IS, Vanag VK. New type of excitatory pulse coupling of chemical oscillators via inhibitor. Physical Chemistry Chemical Physics 2015;17(27):17906-17913.

5. Li Z, Guo Z, Wang M, et al. Firing activities induced by memristive autapse in Fitzhugh–Nagumo neuron with time delay. AEU - International Journal of Electronics and Communications 2021;142:153995.
6. Wu HG, Bao BC, Liu Z, et al. Chaotic and periodic bursting phenomena in a memristive Wien-bridge oscillator. Nonlinear Dynamics 2016;83:893-903.
7. Han XJ, Jiang B, Bi QS. Analysis of the fast-slow hyperchaotic Lorenz system. Acta Physica Sinica 2009;58(9):6006-6015.
8. Bi Q, Chen X, Zhang Z, et al. Nonlinear behaviors as well as the mechanism in a piecewise-linear dynamical system with two time scales. Nonlinear Dynamics 2016;85:2233-2245.
9. Rinzel J. Bursting oscillations in an excitable membrance model. Berlin: Springer 1985;304-316.
10. Naz S, Raja MAZ, Mehmood A, et al. Neuro-intelligent networks for Bouc–Wen hysteresis model for piezostage actuator. The European Physical Journal Plus 2021;136(4):1-20.
11. Xu Q, Li Y. Dahl model-based hysteresis compensation and precise positioning control of an XY parallel micromanipulator with piezoelectric actuation. Journal of dynamic systems, measurement, and control 2010;132(4).
12. Audusse E, Bristeau MO, Perthame B, et al. A multilayer Saint-Venant system with mass exchanges for shallow water flows. Derivation and numerical validation. ESAIM: Mathematical Modelling and Numerical Analysis 2011;45(1):169-200.
13. Bao BC, Yang QF, Zhu L, et al. Chaotic bursting dynamics and coexisting multistable firing patterns in 3D autonomous Morris-Lecar model and microcontroller-based validations. International Journal of Bifurcation and Chaos 2019;29(10):1950134.
14. Proskurkin IS, Vanag VK. Dynamics of a 1D array of inhibitory coupled chemical oscillators in microdroplets with global negative feedback. Phys. Chem. Chem. Phys 2018;20(23):16126-16137.
15. Han XJ, Yu Y, Zhang C. A novel route to chaotic bursting in the parametrically driven Lorenz system. Nonlinear Dynamics 2017;88:2889-2897.
16. Ma XD, Cao SQ. Pitchfork-bifurcation-delayed-induced bursting patterns with complex structures in a parametrically driven Jerk circuit system. Journal of Physics A: Mathematical and Theoretical 2018;51(33):335101.
17. Han XJ, Zhang Y, Bi QS, et al. Two novel bursting patterns in the duffing system with multiple-frequency slow parametric excitations. Chaos 2018;28(4):043111.
18. Wei MK, Jiang W, M XD, et al. Compound bursting dynamics in a parametrically and externally excited mechanical system. Chao, Solitons and Fractals 2021;143:110605.
19. Li XH, Hou JY. Bursting phenomenon in a piecewise mechanical system with parameter perturbation in stiffness. Int. J. Non-Lin. Mech 2016;81:165-176.
20. Zhang ZD, Liu YN, Li J, Bi QS. Bursting oscillations and mechanism of sliding movement in piecewise Filippov system. Acta Phys. Sin 2018;67:40-49.
21. Peng M, Zhang ZD, Qu ZF, Bi QS. Mixed-mode oscillations and the bifurcation mechanism for a Filippov-type dynamical system. Pramana-J. Phys 2019;94:1-10.
22. Qu ZF, Zhang ZD, Peng M, Bi QS. Non-smooth bursting analysis of a Filippov-type system with multiple-frequency excitations. Pramana-J. Phys 2018;91:1-10.
23. Zhang R, Peng M, Zhang ZD, Bi QS. Bursting oscillations as well as the bifurcation mechanism in a non-smooth chaotic geomagnetic field model. Chin. Phys. B 2018;27:416-422.

24. Leutcho GD, Kengne J, Negou AN, et al. A modified simple chaotic hyperjerk circuit: coexisting bubbles of bifurcation and mixed-mode bursting oscillations. Zeitschrift für Naturforschung A 2020;75(7):593-607.
25. Leutcho GD, Kengne J, Kengne LK, et al. A novel chaotic hyperjerk circuit with bubbles of bifurcation: mixed-mode bursting oscillations, multistability, and circuit realization. Physica Scripta 2020;95(7):075216.
26. Li ZJ, Zeng YC. A memristor chaotic circuit based on Wien-bridge oscillator. Journal of Electronics & Information Technology 2014;36(1):88-93.
27. Yu F, Zhang Z, Shen H, et al. FPGA implementation and image encryption application of a new PRNG based on a memristive Hopfield neural network with a special activation gradient. Chinese Physics B 2022;31(2):020505.
28. Ma ML, Yang Y, Qiu ZC, et al. A locally active discrete memristor model and its application in a hyperchaotic map. Nonlinear Dynamics 2022;107:2935-2949.
29. Peng Y, He S, Sun K. A higher dimensional chaotic map with discrete memristor. AEU - International Journal of Electronics and Communications 2021;129:153539.
30. Ding K, Rostami Z, Jafari S, et al. Investigation of cortical signal propagation and the resulting spatiotemporal patterns in memristor-based neuronal network. Complexity 2018;20:6427870.
31. Chen M, Qi JW, Xu Q, et al. Quasi-period, periodic bursting and bifurcations in memristor-based FitzHugh-Nagumo circuit. AEU-International Journal of Electronics and Communications 2019;110:152840.
32. Lin HR, Wang CH, Sun YC, et al. Firing multistability in a locally active memristive neuron model. Nonlinear Dynamics 2020;100:3667-3683.
33. Lin HR, Wang CH, Hong QH, et al. A multi-stable memristor and its application in a neural network. IEEE Transactions on Circuits and Systems II: Express Briefs 2020;67(12):3472-3476.
34. Wang CH, Lin HR, Sun JR, et al. Research Progress on Chaos, Memory and Neural Network Circuits Based on Memristor. Journal of Electronics and Information Technology 2020;42(4):795-810.
35. Wen ZH, Li ZJ, Li X. Bursting dynamics in parametrically driven memristive Jerk system. Chinese Journal of Physics 2020;66:327-334.
36. Zhang ZD, Liu Y, Li J, et al. Bursting ocillations and mechanism of sliding movement in piecewise Filippov system. Acta Physica Sinica 2018;67(11):110501.
37. Cristiano R, Carvalho T, Tonon D J, et al. Hopf and Homoclinic bifurcations on the sliding vector field of switching systems in R3: A case study in power electronics. Physica D 2017;347:12-20.
38. Zhang ZD, Li J, Liu Y, et al. The evolution mechanism of different forms of bursting oscillations in non-smooth dynamical systems. SCIENTIA SINICA Technologica 2019;49(9):1031-1039.
39. Krupa M, Wechselberger M. Local analysis near a folded saddle-node singularity. Journal of Differential Equations, 2010, 248(12): 2841-2888.
40. Kristiansen KU, Hogan SJ. Regularizations of two-fold bifurcations in planar piecewise smooth systems using blowup. SIAM Journal on Applied Dynamical Systems, 2015, 14(4): 1731-1786.
41. Leine RI, Van Campen DH. Bifurcation phenomena in non-smooth dynamical systems. European Journal of Mechanics-A/Solids 2006;25(4):595-616.
42. Qu R, Wang Y, Wu G, et al. Bursting Oscillations and the Mechanism with Sliding Bifurcation in a Filippov Dynamical System. International Journal of Bifurcation and Chaos 2018;28(12): 1850146-18501457.

43. Wang Z, Zhang Z, Bi Q. Bursting oscillations with delayed C-bifurcation in a modified Chua's circuit. Nonlinear Dynamics 2020;100(3):2899-2915.